Multi-objective optimization of curved composite laminated plates

Fábio Miguel Cascalheira Aguincha

fabio.aguincha@tecnico.ulisboa.pt

Instituto Superior Técnico, Universidade de Lisboa, Portugal

December 2019

The increasing use of carbon fiber composite materials is due, among other reasons, to their low weight, high stiffness and good fatigue behavior. By hybridizing carbon fiber composites with the addition of glass fibers, it is possible to create new lightweight composite materials that are simultaneously more ductile, more impact resistant and have a lower associated cost and may have many applications in structural components. Experimental tests were performed to determine the displacements of curved plates in laminated hybrid composite material when submitted to flexion-torsion loads. The plates were produced with different lamination configurations using hand lay-up, with carbon fiber and glass fiber reinforcements in an epoxy resin matrix. The elastic properties of the blades were obtained through tensile tests applied to specimens manufactured with the referred fibers. The computational simulations of the experimental tests were performed in Abaqus. The results of these simulations were analysed and compared with the experimental results. Plate optimization was performed using DMS, a multi-objective, direct search optimization method. The objective functions were the minimization of the maximum value of plate displacement, mass and cost that were obtained through a cycle interaction between DMS and Abaqus. Finally, three solutions best suited to the problem objectives were obtained.

Keyword: Hybrid composites, carbon and glass fibers, multi-objective optimization, finite element method.

1 Introduction

Polymer matrix laminate composite materials have been increasingly used in various structural applications due to their high stiffness and specific strength. In particular, in the aerospace industry a large percentage of the composite materials used in structural components are carbon fiber reinforced polymers. However, due to their high strength and high modulus of elasticity, carbon fibers are quite brittle compared to other composite reinforcements, exhibiting low toughness values [1]. Increasing toughness of continuous fiber reinforced composite materials has been an area of much research and development in the scientific community. Several strategies have been developed to make these materials more ductile and more impact resistant. The rupture strain values of these materials can be greatly increased by replacing some of the brittle fibers with more ductile fibers [2]. Due to the need to create new lightweight composite materials without compromising their toughness, there has emerged an interest in the hybridization of carbon fiber composites with the addition of glass fibers [3]. When building a new composite material through this hybridization, the goal is to retain the advantages of carbon and glass fibers while eliminating their major disadvantages [4]. In addition, in a laminated composite material, replacing carbon fiber layers in the laminate with glass fiber layers reduces the cost of this material, makes it more impact resistant, and hardly changes its flexural properties [5].

2   Description of numerical models

Two curve composite plates were modelled in ABAQUS [6], with different configurations in the laminate (different number, material arrangement and orientations of layers). After obtaining the numerical results, these were compared to the results of several mechanical tests, which were performed in the same conditions as the ones in the models created, in order to validate said models.

2.1   Geometry, boundary conditions and FE mesh

The dimensions of the plates are presented in Figure 1a and the model's boundary conditions are illustrated in Figure 1b. The plates are fixed in one end and there is a concentrated load F, with the value of 44 N. Both displacements, U_d and U_e are considered positive in the same sense as the load vector.

As previously said, two types of plates were modelled, and each configuration can be found in Table 1. In the material distribution, carbon fibers are indicated by the letter C, while the glass fibers are indicated by the letter G.

The same mesh was generated for both plates and can be seen in Figure 2. This mesh is composed of 600 elements of type S8R [6].
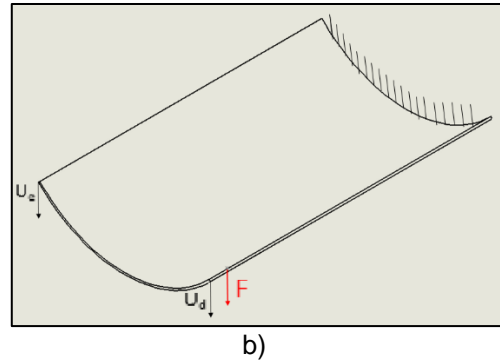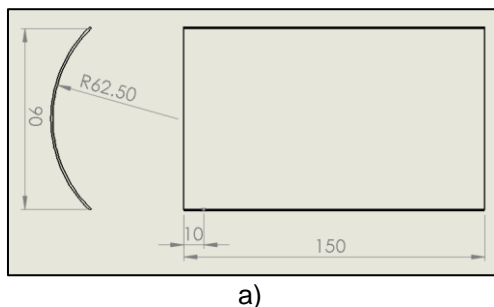

a)

b)

Figure 1 - a) Plate dimensions [mm]; b) boundary conditions

Table 1 – Configurations of both plates.

Plate	No. of layers	Material Distribution	Layer orientations
A	6	G / C / G / G / C / G	$[90_2/0/90/0_2]$
B	8	G / C / C / G / G / C / C / G	$[0_2/90_2]_S$

2.2   Material properties

The materials that constitute the layers of the plates are carbon fibers and glass fibers. The mechanical properties of each material are presented in Table 2 (E_i – Young's modulus, v_{ij} – Poisson's coefficient, G_{ij} – shear modulus, S_{ti} – tensile strength, S_{ci} – compressive strength, S_{sij} – shear strength, G_f – fracture energy). The mechanical properties are referred to local material directions (i, j = 1, 2 or 3) and we have 1=Z, 2=X and 3=Y (X, Y, Z – Figure 2).

Table 2 - Material properties [7] [8] [9].

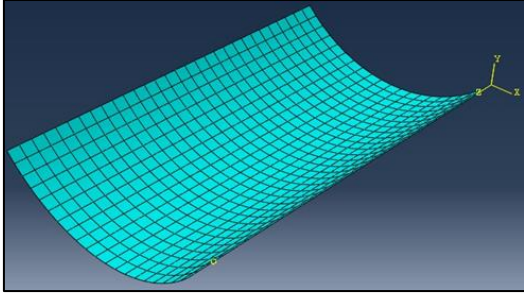|	Carbon fiber	Glass fiber
E_1 [MPa]	91070	27128
E_2 [MPa]	10000	2542
v_{12}	0.3	0.25
$G_{12} = G_{13}$ [MPa]	5000	4000
G_{23} [MPa]	3470	3211
S_{t1} [MPa]	1500	1000
S_{c1} [MPa]	1200	600
S_{t2} [MPa]	50	30
S_{c2} [MPa]	250	110
$S_{s12} = S_{s23}$ [MPa]	75	40
G_{ft} [N/mm]	5.86	2.38
G_{fc} [N/mm]	5.42	5.28
G_{mt} [N/mm]	0.424	0.424
G_{mc} [N/mm]	0.948	0.948
Thickness [mm]	0.3	0.53

Figure 2 - FE mesh of the plate model.

2.3 Hashin damage criterion

The Hashin damage criterion is based on the works of Hashin and Rotem [10] and Hashin [11]. Unlike the polynomial criteria such as the Tsai-Hill and Tsai-Wu criteria [12] [13], which propose a single equation to predict damage initiation, the Hashin damage criterion takes into account four possible failure modes with four corresponding indexes: fiber breakage in tension, fiber buckling in compression, matrix racking in tension and matrix crushing in compression. According to the previous failure modes the four following equations apply, respectively:

$$F_f{}^t = \left(\frac{\sigma_{11}}{S_{t1}}\right)^2 + \left(\frac{\sigma_{12}}{S_{s12}}\right)^2 \tag{1}$$

$$F_f{}^c = \left(\frac{\sigma_{11}}{S_{c1}}\right)^2 \tag{2}$$

$$F_m{}^t = \left(\frac{\sigma_{22}}{S_{t2}}\right)^2 + \left(\frac{\sigma_{12}}{S_{s12}}\right)^2 \tag{3}$$

$$F_m{}^c = \left(\frac{\sigma_{22}}{2S_{S23}}\right)^2 + \left[\left(\frac{S_{c2}}{2S_{S23}}\right)^2 - 1\right]\frac{\sigma_{22}}{S_{c2}} + \left(\frac{\sigma_{12}}{S_{s12}}\right)^2 \tag{4}$$

where σ_{11}, σ_{22} and σ_{12} are the applied stresses and S_{ti}, S_{ci} and S_{sij} have the meaning previously explained.

If one of the indexes exceeds the value of 1.0 it means that the damage has begun in the material in one of the corresponding modes referred. Once damage initiation criteria has been satisfied in a given element, it is not able to support all the stress and therefore $\hat{\sigma}$, effective stress tensor, intends to represent the stress acting over the damaged area that effectively resists the internal forces. Therefore this tensor is given by:

$$\hat{\sigma} = \sigma M \text{ where } M = \begin{bmatrix} \frac{1}{(1-d_f)} & 0 & 0 \\ 0 & \frac{1}{(1-d_m)} & 0 \\ 0 & 0 & \frac{1}{(1-d_s)} \end{bmatrix} \tag{5}$$

In equation 5, σ is the true stress and M is the damage operator. d_f, d_m and d_s are internal variables that characterize fibre,

matrix and shear damage, which are associated with the previous four modes mechanisms:

$$d_f = \begin{cases} d_f{}^t & if \ \sigma_{11} \geq 0 \\ d_f{}^c & if \ \sigma_{11} < 0 \end{cases} \tag{6}$$

$$d_m = \begin{cases} d_m{}^t & if \ \sigma_{22} \geq 0 \\ d_m{}^c & if \ \sigma_{22} < 0 \end{cases} \tag{7}$$

$$d_s = 1 - (1 - d_f{}^t)(1 - d_f{}^c)(1 - d_m{}^t)(1 - d_m{}^c) \tag{8}$$

Before the damage initiates the material is in linear elastic regime and, in that case, M corresponds to the identity matrix. Once damage initiation criteria is verified for any mode, there is a reduction in stiffness matrix values, and the constitutive law is given by:

$$\sigma = C_d \varepsilon \tag{9}$$

$$D = 1 - (1 - d_f)(1 - d_m)v_{12}v_{21} \tag{10}$$

$$C_d = \frac{1}{D}\begin{bmatrix} (1-d_f)E_1 & (1-d_f)(1-d_m)v_{12}E_1 & 0 \\ (1-d_f)(1-d_m)v_{12}E_2 & (1-d_m)E_2 & 0 \\ 0 & 0 & (1-d_s)GD \end{bmatrix} \tag{11}$$

where ε is the strain and C_d represents the damaged elasticity matrix.

3 Numerical and experimental results and comparison

In order to validate the models developed in this work, two plates were manufactured using the Hand Lay-Up method (plates A and B) and were then submitted to bending-torsion experimental tests in the boundary conditions mentioned in section 2.1. The displacements U_d and U_e were measured several times through several tests and the average of the results was found. Both the results of the numerical analyses and the experimental tests were compared in order to validate the models developed. Both results are shown in Table 3. The error was calculated as a percentage according to the following formula:

$$\Delta = abs\left(\frac{displacement_{experimental} - displacement_{Abaqus}}{displacement_{experimental}}\right) * 100 \tag{12}$$

It can be expected that U_d and U_e show symmetrical signals (positive U_d and negative U_e), since the load applies bending and torsion on the plates (in addition to shear stress). Regarding the differences between the experimental and numerical values, it is noteworthy that the displacement values U_d have relatively low error values, with the lowest value (3.88%) to be recorded on plate

A. For displacement U_e, the error values are higher than expected, with the numerical value almost double the experimental value (88.08%) in the worst case. This discrepancy is due to the fact that the plates were warped after being cut to the desired shape, and because of this warping, only the edge corresponding to the displacement U_d could be guaranteed to be horizontal during the experimental tests carried out, so it should be expected that the recorded experimental U_e values would in fact be different from those obtained numerically. Nevertheless, it can be seen that the computational model developed was accurate in predicting the mechanical behaviour of the plate's displacements.

Table 3 – Difference between the experimental and numerical results.

		Experimental displacement [mm]	*Abaqus* displacement [mm]	Δ %
Plate A	U_d	2.962	2.847	3.88
	U_e	-0.814	-1.531	88.08
Plate B	U_d	1.706	1.571	7.91
	U_e	-0.552	-0.786	42.39

4 Optimization method and application

4.1 Direct MultiSearch (DMS) method

A constrained nonlinear multiobjective optimization problem can be mathematically formulated as

$$\min \ F(x) \equiv (f_1(x), f_2(x), \dots, f_m(x))^T \quad (13)$$
$$\text{s.t. } x \in \Omega$$

involving m objective functions.

In the presence of m (≥2) objective functions, the minimizer of one function is not necessarily the minimizer of another. In this case, we don't have a single point that yields the "optimum point for all objectives". Instead, we have a set of points, called Pareto optimal or non-dominated set. Given two points x_1, x_2 in Ω, x_1 is said to dominate, in Pareto sense, another point x_2 if and only if solution x_1 is strictly better than x_2 in at least one of the objectives and point x_1 is not worse than x_2 in any of the objectives. A set of points in Ω is non-dominated when no point in the set is dominated by another one in the set.

Direct MultiSearch (DMS) [14] is a solver for multiobjective optimization problems, without the use of derivatives and does not aggregate any components of the objective function. It essentially generalizes all direct-search methods of directional type from single to multiobjective optimization. DMS maintains a list of feasible non-dominated points (from which the new iterates or poll centres are chosen). DMS tries, however, to capture the whole Pareto front from the polling procedure itself. At each iteration, the new feasible evaluated points are added to this list and the dominated ones are removed. Successful iterations correspond then to changes in the iterate list, meaning that a new feasible non-dominated point was found. Otherwise, the iteration is declared as unsuccessful.

Most of the details have been omitted in this brief explanation, but the full description of the algorithm can be found in reference [28]. During this, the default parameters that come with DMS were used.

4.2 Objectives and design variables

In this work there are 3 objectives to minimize: plate's mass, plate's cost and the maximum displacement of the plate (U_d). In multiobjective optimization, it is important that the objective functions are contradictory, which means that while minimizing one of the objectives, the minimization of the others is not guaranteed. In this particular work the opposite objectives are mass and cost, because due to the materials used (glass fiber and carbon fiber) the lighter the plate is the more expensive it will be and vice versa. This is because carbon fiber is a lighter material than glass fiber but also more expensive. So by minimizing the mass of the structure, its cost will be increased.

The design variables in this optimization are the number of layers in the plate, the orientations of each layer and the material of each layer. Some restrictions have been imposed on the problem. The number of layers ranges from 6 to 12, so as not to get a very thin plate and to have an upper limit of plate thickness. If there is no maximum number of layers, minimizing displacement could lead to results with a very high number of layers. An angle range

for layer orientation between -75⁰ and 90⁰ with a 15⁰ step was also defined. With this range of variation of orientation angles, this design variable can take the values of {-75⁰, -60⁰, -45⁰, -30⁰, -15⁰, 0⁰, 15⁰, 30⁰, 45⁰, 60⁰, 75⁰, 90⁰}. The value of -90⁰ was not included because a fiber with this orientation value exhibits the same mechanical behaviour as a fiber at 90⁰. As for the material, the layers can only be carbon fiber or glass fiber, as they were the 2 materials used throughout the work. The thickness of each layer material is the same as stated in Table 2.

4.3   Application

Since DMS uses variables with real values and this problem has variables with discrete values, we consider a vector of variables with 25 entries:

$$x = [x_1, x_2, ..., x_{25}]^T \qquad (14)$$
$$\text{s. t.} \quad x \in \Omega$$

The first entry x_1 corresponds to the number of layers in the plate and, as previously mentioned, ranges from 6 to 12. The next 12 entries $[x_2: x_{13}]$ correspond to the orientations of the layers and, as previously mentioned, range from -75 to 90, with a step of 15. The last 12 variables $[x_{14}: x_{25}]$ correspond to the materials of the layers and can take the value 1 or 2. The value 1 corresponds to carbon fiber and the value 2 corresponds to glass fiber. It is important to note that if the value of x_1 is, for example 6 (6 layers), this means that only the values of $[x_2: x_7]$ and $[x_{14}: x_{19}]$ will be considered for analysis and the remaining variables are assumed to be null.

5   Results and discussion

The obtained solution is illustrated in Figure 3a. This Pareto front has a total of 70 non-dominated points. In order to be able to discuss the results, 3 different projections of the points in different planes are presented: mass-cost, mass-displacement and cost-displacement, as shown in Figure 3b, c and d, respectively. In these, some of the non-dominated points are highlighted and the respective configurations and values of the objectives for these points are mentioned in Table 4 to compare solutions.

Figure 3b shows 4 solutions to illustrate mass-cost variation. Solution 68 is the best in terms of mass (39.24 g), while solution 70 is the best in terms of cost (1.22 €). As expected, solution 68 is entirely made of carbon fiber and solution 70 is made entirely of glass fiber and both have the minimum number of layers. Solutions 2 and 3 are intermediate configurations.

Figure 3c shows 4 solutions to illustrate mass-displacement variation. Solution 10 is the best in terms of displacement (0.25 mm). As expected, this solution has the maximum number of layers. This allows for low displacement values but makes this solution one of the worst in mass (the worst has 161.2 g). Solution 68 remains the best in terms of mass, but as it turns out it is the worst solution in terms of displacement values (1.91 mm). Solutions 54 and 56 are intermediate configurations having slightly higher displacement values than solution 10 but having much smaller mass values.

Figure 3d shows 4 solutions to illustrate the displacement-cost variation. Solution 10 remains the best in terms of displacement values and as it turns out has a relatively low cost value over the most expensive solution (9.6 €). Solution 70 has one of the highest displacement values between the solutions found. Solutions 64 and 67 are intermediate configurations which have slightly higher displacement values than solution 10 but are much more economical.

After looking at the best solutions for each objective and isolating a few intermediate configurations for each objective plane, there are other approaches that can be used to try to find a solution that is most desired. One possible approach is to consider a pseudo objective, that is, isolate the best solutions to the original 3 goals and use the values of a fourth goal to help decide the "optimal solution". In this work, it was decided to use as a fourth objective the load necessary to bring the plate to failure under load. For this the Hashin failure criterion is used. The initial intention would be to use this load as the fourth objective directly in the optimization cycle described, but because this objective significantly increased the analysis time (about 200 times more) it was decided to use only 3 objectives in the optimization.

Table 4 – Configurations and values of the objectives of the non-dominated points in Figure 3.

| Point	No. of layers	Material distribution	Layer orientation	Mass [g]	Cost [€]	Displacement [mm]
2	6	$[C_2G_3C]$	$[-45/15/0_2/30/-45]$	59.91	3.01	1.34
3	6	$[C_2G]_S$	$[-45/15/0_2/30/-45]$	53.02	3.61	1.45
10	12	$[C_2G_4]_S$	$[-30/-45/30/15_2/0_2/15/0/45/-30/-45]$	133.6	4.83	0.25
54	12	$[C_{12}]$	$[-45_2/30/15/-15/0_2/15/0/45/-45_2]$	78.48	9.6	0.39
56	11	$[C_{11}]$	$[-45_2/30/15_2/0_3/-45/45/-45]$	71.94	8.8	0.48
64	12	$[G_{12}]$	$[-30/-45/30/15_2/0_4/45/-30/-45]$	161.2	2.45	0.31
67	11	$[G_{11}]$	$[-30/-45/30/15/0_4/30/-30_2]$	147.7	2.24	0.38
68	6	$[C_6]$	$[-45/15/0_2/30/-45]$	39.24	4.8	1.91
70	6	$[G_6]$	$[-45/30/0_2/30/-45]$	80.58	1.22	1.54
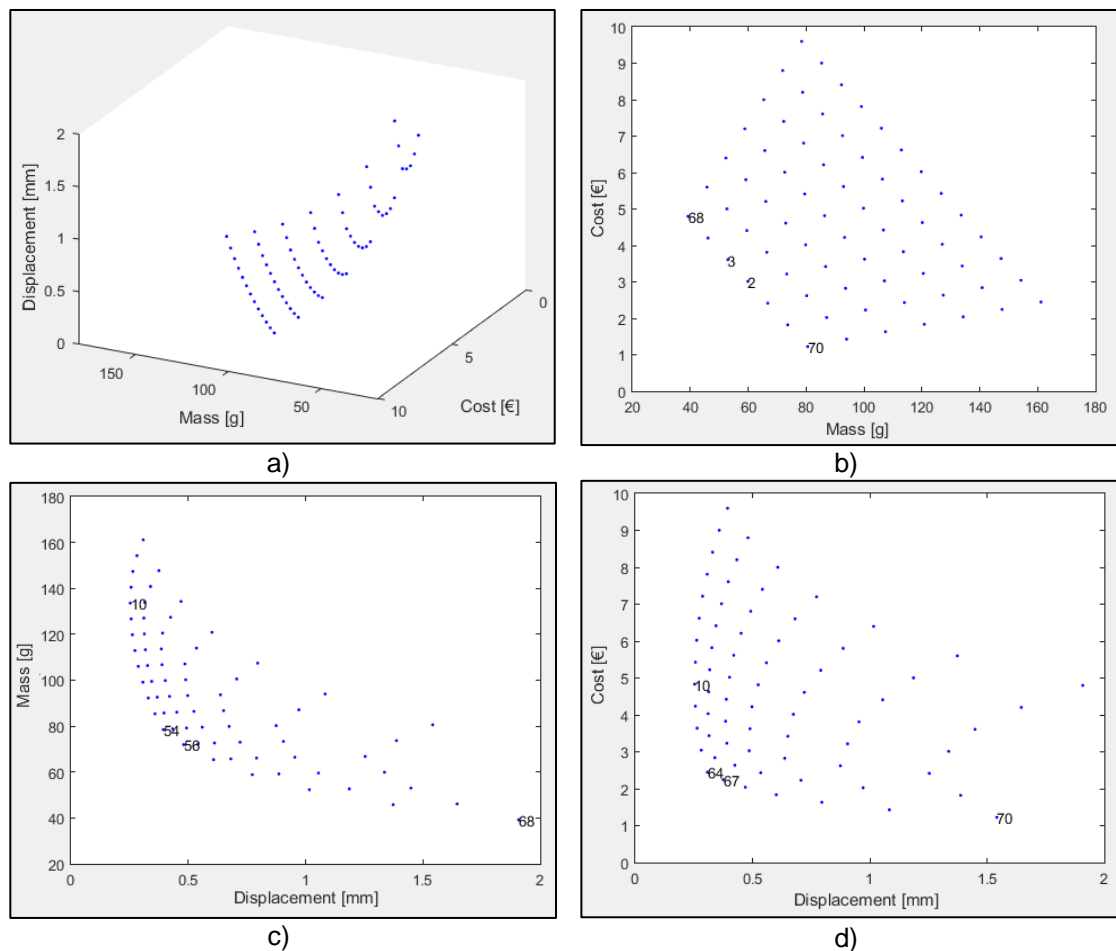
Figure 3 - Four different perspectives of visualization to the same set of non-dominated solutions: a) showing all planes; b), c) and d) presenting three projections in the planes mass-cost, displacement-mass and displacement-cost, respectively.

The best solution for each objective and 3 intermediate configurations were chosen for the simulations with implementation of the Hashin criterion. For this, we select the solution that has the best value of the objective that is not present in the plane projections indicated. For example, for mass-cost projection, we choose the intermediate solution with the best displacement value. Given this, the solutions chosen for these simulations were solutions 2, 10, 56, 67, 68 and 70.

These simulations are similar to those described previously, with one difference. Instead of a concentrated load, there is a boundary condition in U_d of vertical displacement (-50 mm). The load-displacement graphs of the solutions used are shown in Figure 4. The point where there is an abrupt change of slope in these graphs is the point at which the material fails and the load at that point corresponds to the fourth objective defined. Table 5 shows the values of the loads where the failure occurred, the values of the displacements where the failure occurred, the stiffness and the corresponding failure modes.

Table 5 - Stiffness and failure load, displacement and mode of the points analysed.

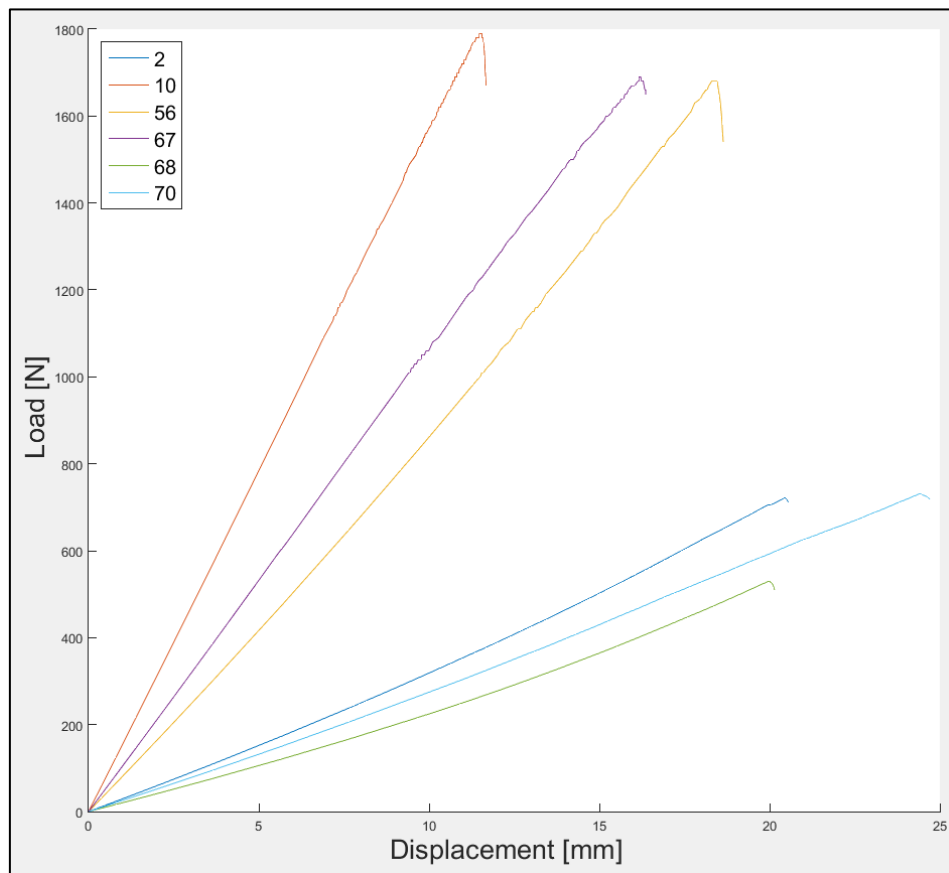| Point	Failure load [N]	Failure displacement [mm]	Stiffness [N/mm]	Failure mode
2	721	20.44	37.59	CM
10	1787	11.54	155.56	CM
56	1681	18.40	93.31	CM
67	1685	16.21	103.93	CM
68	529	19.99	27.41	TM
70	730	24.44	30.99	CM

Figure 4 – Load-displacement graphs for the points evaluated.

As expected, all plates had the damage initiation in the matrix. The matrix is the weakest component so it was expected that the damage would start on it. All solutions had damage start in matrix compression mode (CM), except solution 68, which initiated damage with matrix tensile stress (TM). In terms of failure load, the solution with the highest (most desired) load value is solution 10, with a value of 1787 N, also presenting the highest stiffness (155.56 N / mm). However, solutions 56 and 67 have failure load values that are not much lower than solution 10's values with fairly acceptable stiffness values when compared to other solutions. Also add the fact that both solutions 56 and 67 have greater ductility than solution 10. If we want to determine an optimal solution, we can opt for solution 10, as this is the best in terms of performance with the smallest displacement and highest failure load and stiffness value. However, if we need to choose more economical or lighter options without losing much in performance, we can choose either solution 56 (lighter than 10) or solution 67 (lower cost than 10).

From this application it becomes clear that the multiobjective optimization approach allows for a great flexibility in the design process. The need to conduct several single objective optimizations during the design process is thus kept to a minimum due to the fact that the available non dominated solutions can always be analysed from several perspectives.

6   Conclusions

In this work we apply the Direct MultiSearch for the design of composite curve plate. The plate is designed for minimum displacement, mass and material cost, by choosing the number of layers, the material of the layers, as well as the respective orientations. The solutions are presented in the form of a Pareto trade-off front and the results are analysed using the projections of this Pareto surface. The obtained results can be very useful in the design of this kind of structures, where a compromise between weight reduction, material cost and the value of displacement is sought.

References

[1] P. W. Manders e M. G. Bader, "The strength of hybrid glass/carbon fibre composites," *Journal of Materials Science,* vol. 16, pp. 2246-2256, 1981.

[2] A. R. Bunsell e B. Harris, "Hybrid carbon and glass fibre composites," *Composites,* vol. 5, pp. 157-164, 1974.

[3] M. R. Wisnom, G. Czél, Y. Swolfs, M. Jalalvand, L. Gorbatikh e I. Verpoest, "Hybrid effects in thin ply carbon/glass unidirectional laminates: accurate experimental determination and prediction," *Composites Part A: Applied Science and Manufacturing,* vol. 88, pp. 131-139, 2016.

[4] G. Kretsis, "A review of the tensile, compressive, flexural and shear properties of hybrid fibre-reinforced plastics," *Composites,* vol. 18, pp. 13-23, 1987.

[5] Y. Swolfs, L. Gorbatikh e I. Verpoest, "Fibre hybridisation in polymer composites : A review," *Composites Part A: Applied Science and Manufacturing,* vol. 67, pp. 181-200, 2014.

[6] Simulia, *ABAQUS/Standard User's Manual, Version 6.14,* Providence, RI, USA: Dassault Systèmes, 2014.

[7] Performance Composites Ltd, "Mechanical Properties of Carbon Fibre Composite Materials, Fibre / Epoxy resin (120ºC)," [Online]. Available: http://www.performance-composites.com/carbonfibre/mechanicalproperties_2.asp. [Accessed in June 2019].

[8] P. Krishnan, "Vibrations and fatigue interactions of laminate composites, p. Slide 59 e 60.," [Online]. Available: https://pt.slideshare.net/PadmanabhanKrishnan2/vibrations-and-fatigue-vibration-interactions-of-laminated-composites. [Accessed in June 2019].

[9] F. Nunes, J. R. Correia e N. Silvestre, "Structural behavior of hybrid FRP pultruded beams: Experimental, numerical and analytical studies," *Thin-Walled Structures,* vol. 106, pp. 201-217, 2016.

[10] Z. Hashin e A. Rotem, "A Fatigue Failure Criterion for Fiber Reinforced Materials," *Journal of Composite Materials,* vol. 7, pp. 448-464, 1973.

[11] Z. Hashin, "Failure Criteria for Unidirectional Fiber Composites," *Journal of Applied Mechanics,* vol. 47, pp. 329-334, 1980.

[12] S. W. Tsai, "Strength Characteristics of Composite Materials," Philco Corporation, Newport Beach, CA, USA, 1965.

[13] S. W. Tsai e E. M. Wu, "A General Theory of Strength for Anisotropic Materials," *Journal of Composite Materials,* vol. 5, pp. 58-80, 1971.

[14] A. L. Custódio, . J. A. Madeira, A. I. Vaz e L. N. Vicente, "Direct multisearch for multiobjective optimization," *SIAM Journal on Optimization,* vol. 21, pp. 1109-1140, 2011.